

# Divergent polo boxes in KKT2 bind KKT1 to initiate the kinetochore assembly cascade in *Trypanosoma brucei*

Midori Ishii<sup>†</sup>, Patryk Ludzia<sup>†</sup>, Gabriele Marcianò<sup>†</sup>, William Allen, Olga O. Nerusheva, and Bungo Akiyoshi\*

Department of Biochemistry, University of Oxford, Oxford, OX1 3QU, UK

**ABSTRACT** Chromosome segregation requires assembly of the macromolecular kinetochore complex onto centromeric DNA. While most eukaryotes have canonical kinetochore proteins that are widely conserved among eukaryotes, evolutionarily divergent kinetoplastids have a unique set of kinetochore proteins. Little is known about the mechanism of kinetochore assembly in kinetoplastids. Here we characterize two homologous kinetoplastid kinetochore proteins, KKT2 and KKT3, that constitutively localize at centromeres. They have three domains that are highly conserved among kinetoplastids: an N-terminal kinase domain of unknown function, the centromere localization domain in the middle, and the C-terminal domain that has weak similarity to polo boxes of Polo-like kinases. We show that the kinase activity of KKT2 is essential for accurate chromosome segregation, while that of KKT3 is dispensable for cell growth in *Trypanosoma brucei*. Crystal structures of their divergent polo boxes reveal differences between KKT2 and KKT3. We also show that the divergent polo boxes of KKT3 are sufficient to recruit KKT2 in trypanosomes. Furthermore, we demonstrate that the divergent polo boxes of KKT2 interact directly with KKT1 and that KKT1 interacts with KKT6. These results show that the divergent polo boxes of KKT2 and KKT3 are protein-protein interaction domains that initiate kinetochore assembly in *T. brucei*.

## Monitoring Editor

Kerry Bloom  
University of North Carolina,  
Chapel Hill

Received: Jul 11, 2022

Revised: Sep 9, 2022

Accepted: Sep 14, 2022

## INTRODUCTION

The kinetochore is the macromolecular protein complex that drives chromosome segregation in eukaryotes (McIntosh, 2016). It assembles onto centromeric DNA and interacts with spindle microtubules during mitosis and meiosis. In most eukaryotes, the position of kinetochore assembly sites is marked by the presence of a centromere-specific histone H3 variant, CENP-A, which also plays important roles in the recruitment of other kinetochore proteins (Musacchio and Desai, 2017). CENP-A is found in diverse eukaryotes, suggesting that most eukaryotes use CENP-A to initiate the kinetochore

assembly cascade (Drinnenberg and Akiyoshi, 2017; van Hooff *et al.*, 2017). However, CENP-A is absent in some lineages such as kinetoplastids, holocentric insects, and early-diverging fungi, implying that there are alternative mechanisms for kinetochore assembly (Drinnenberg *et al.*, 2014; Navarro-Mendoza *et al.*, 2019; Ishii and Akiyoshi, 2022).

Kinetoplastids are flagellated eukaryotes defined by the presence of a unique organelle called the kinetoplast that contains a cluster of mitochondrial DNA (d'Avila-Levy *et al.*, 2015). They are evolutionarily

This article was published online ahead of print in MBoc in Press (<http://www.molbiolcell.org/cgi/doi/10.1091/mbc.E22-07-0269-T>) on September 21, 2022.  
Competing financial interests: The authors declare no competing financial interests.

Author contributions: M.I. performed LacO–LacI tethering, RNAi, and rescue experiments in trypanosomes. P.L. purified various recombinant proteins, identified interaction between KKT1C and KKT2 DPB, and performed cross-linking mass spectrometry. P.L. and W.A. solved the KKT2 DPB crystal structure. G.M. solved the KKT3 DPB crystal structure. O.O.N. made analog-sensitive KKT2 and KKT3 alleles as well as KKT3 mutants. B.A. performed in vitro kinase assays and immunoprecipitation of KKT1 fragments from trypanosomes. B.A. wrote the manuscript. M.I., P.L., and G.M. edited the manuscript.

Rights retention: This research was funded in whole or in part by Wellcome Trust (grant 210622/Z/18/Z). For the purpose of Open Access, the author has applied a CC BY public copyright license to any Author Accepted Manuscript (AAM) version arising from this submission.

\*Address correspondence to: Bungo Akiyoshi ([bungo.akiyoshi@bioch.ox.ac.uk](mailto:bungo.akiyoshi@bioch.ox.ac.uk)).

<sup>†</sup>These authors contributed equally to this work.

Abbreviations used: DPB, divergent polo box; PLK, Polo-like kinase.

© 2022 Ishii *et al.* This article is distributed by The American Society for Cell Biology under license from the author(s). Two months after publication it is available to the public under an Attribution–Noncommercial–Share Alike 4.0 International Creative Commons License (<http://creativecommons.org/licenses/by-nc-sa/4.0>). “ASCB®,” “The American Society for Cell Biology®,” and “Molecular Biology of the Cell®” are registered trademarks of The American Society for Cell Biology.

divergent from traditional model eukaryotes used in kinetochore research, such as yeasts, worms, flies, and humans (Keeling and Burki, 2019). Interestingly, none of the canonical kinetochore proteins, including CENP-A, have been found in the genome of kinetoplastids (Lowell and Cross, 2004; Berriman *et al.*, 2005; van Hooff *et al.*, 2017). Instead, experimental studies in *Trypanosoma brucei* have identified unique kinetochore proteins called KKT1–25 (Akiyoshi and Gull, 2014; Nerusheva and Akiyoshi, 2016; Nerusheva *et al.*, 2019) and KKIP1–12 (D'Archivio and Wickstead, 2017; Brusini *et al.*, 2021), many of which are conserved in kinetoplastids (Butenko *et al.*, 2020; Geoghegan *et al.*, 2021). Dissecting the unique kinetoplastid kinetochores can provide insights into the evolution and fundamental requirements of chromosome segregation in eukaryotes. Based on architectural similarities between kinetoplastid kinetochores and synaptonemal complexes, as well as sequence similarities between their components, we proposed that kinetoplastids might have repurposed meiotic synaptonemal complexes and homologous recombination machinery to assemble the unique kinetochore (Tromer *et al.*, 2021).

There are a number of outstanding questions about kinetoplastid kinetochores. For example, it remains unknown how kinetoplastid kinetochores assemble on centromeres. In other eukaryotes, CENP-A-containing nucleosomes recruit components of the constitutive centromere-associated network (CCAN) to initiate the kinetochore assembly cascade. There are six proteins in *T. brucei* that constitutively localize at kinetochores (KKT2, KKT3, KKT4, KKT20, KKT22, and KKT23), and these proteins may form the foundation of kinetoplastid kinetochores (Akiyoshi and Gull, 2014; Nerusheva *et al.*, 2019). Growth defects have been observed upon depletion of KKT2, KKT3, KKT4, and KKT23 (Marcianò *et al.*, 2021). KKT4 has microtubule-binding activity (Llauro *et al.*, 2018), while KKT23 has a GCN5-related N-acetyltransferase domain of unknown function (Nerusheva *et al.*, 2019). Importantly, kinetochore localization of KKT2 and KKT3 was not affected when KKT4 or KKT23 were depleted, while depletion of KKT2 and KKT3 affected the localization of other kinetochore proteins including KKT4 and KKT23 (Marcianò *et al.*, 2021). Together with the finding that KKT2 and KKT3 have DNA-binding motifs (Akiyoshi and Gull, 2014), it is plausible that these constitutive kinetochore proteins form the base of kinetoplastid kinetochores and recruit other kinetochore proteins to initiate the assembly cascade.

KKT2 and KKT3 are homologous to each other and have several domains that are highly conserved among kinetoplastids, including an N-terminal kinase domain, the central domain, and divergent polo boxes (DPB; Figure 1A; Nerusheva and Akiyoshi, 2016). The kinase domains of KKT2 and KKT3 have been classified as unique among eukaryotic kinases (Parsons *et al.*, 2005), and very little is known about the function or substrate of these kinase domains. The central domains of KKT2 and KKT3 localize at kinetochores when ectopically expressed in trypanosomes and were named the centromere localization domain (Marcianò *et al.*, 2021). Polo boxes are protein–protein interaction domains found in Polo-like kinases (PLKs) that often must be phosphorylated to enable protein–protein interactions (Elia *et al.*, 2003; Zitouni *et al.*, 2014). Immunoprecipitation of ectopically expressed KKT2 DPB and KKT3 DPB from trypanosomes revealed copurification of several kinetochore proteins, supporting the possibility that these divergent polo boxes are protein–protein interaction domains that contribute to kinetochore assembly in kinetoplastids (Marcianò *et al.*, 2021). To date, direct interaction partners of the divergent polo boxes remain unknown.

Here we report characterization of the unique kinase domain and divergent polo boxes of KKT2 and KKT3. We show that the kinase

activity of KKT2, but not KKT3, is essential for accurate chromosome segregation in the procyclic (insect) form of *T. brucei*. Crystal structures of their divergent polo boxes confirm similarity to the polo boxes of PLK1 and reveal differences between KKT2 and KKT3. We also show that KKT3's divergent polo boxes can recruit KKT2 in trypanosomes and that KKT2's divergent polo boxes directly interact with KKT1. These results show that KKT2 and KKT3 play key roles in the assembly of kinetoplastid kinetochores by recruiting downstream kinetochore proteins using their divergent polo boxes.

## RESULTS

### KKT2 kinase activity is essential for chromosome segregation

A recent study showed that a kinase-dead allele of KKT2 was unable to support proliferation of the bloodstream form *T. brucei* (Saldivia *et al.*, 2021). To examine the importance of the KKT2 kinase activity in the procyclic (insect) form cells that we have been using for our kinetoplastid kinetochore studies, we created analog-sensitive KKT2 alleles by mutating its gatekeeper residue (M161; Bishop *et al.*, 2000). The cell line carrying KKT2-as2 (M161A) as the sole copy of KKT2 grew normally but had a growth defect upon addition of 1NA-PP1, an analog of the kinase inhibitor PP1 (Figure 1B). Judging from the number of kinetoplasts (K) and nuclei (N) in a cell (Robinson *et al.*, 1995), there was no striking change in the cell cycle profile upon inhibition of the KKT2 kinase activity (Figure 1C). KKT2 localized at kinetochores when its kinase activity was inhibited, but >40% of anaphase cells had lagging kinetochores after an 8-h treatment (Figure 1D). These results show that the kinase activity of KKT2 is essential for proper chromosome segregation in the procyclic form.

We next examined the contribution of KKT2's kinase activity for the localization of other kinetochore proteins. Based on our previous finding that KKT14 failed to localize at kinetochores upon RNAi-mediated depletion of KKT2 (Marcianò *et al.*, 2021), we first monitored the localization of KKT14 but found that it still localized at kinetochores upon inhibition of the KKT2 kinase activity (Figure 1E). KKT1 also localized at kinetochores (Figure 1E). These results show that the kinase activity of KKT2 is essential for accurate chromosome segregation but is dispensable for the localization of itself, KKT1, and KKT14.

### KKT3 kinase activity is dispensable for the proliferation of procyclic cells

Similarly to KKT2, KKT3 is essential for cell growth (Akiyoshi and Gull, 2014; Jones *et al.*, 2014). To our surprise, cells carrying KKT3-as1 (M109G) as the sole copy of KKT3 did not have any growth defect even in the presence of 1NA-PP1, 1NM-PP1, or 3MB-PP1 (see *Materials and Methods*). We next created a kinase-dead allele of KKT3 by mutating lysine 63 (a residue conserved in active protein kinases in eukaryotes) and found that the cell line carrying KKT3<sup>K63A</sup> as the sole copy of KKT3 grew normally without obvious defects (unpublished data). We even obtained a cell line that entirely lacked the kinase domain of KKT3, which segregated chromosomes accurately during anaphase (Figure 1F). These results show that the kinase activity of KKT3 is not essential for cell growth in procyclic cells. Given its high level of sequence conservation, however, it is possible that its kinase activity is essential under certain growth conditions or at certain life stages.

### KKT2 phosphorylates KKT8, while KKT3 phosphorylates KKT12

We next aimed to identify substrates of KKT2 and KKT3 by in vitro kinase assays using recombinant proteins (Supplemental Figure S1A). While screening several kinetochore proteins and histones, we

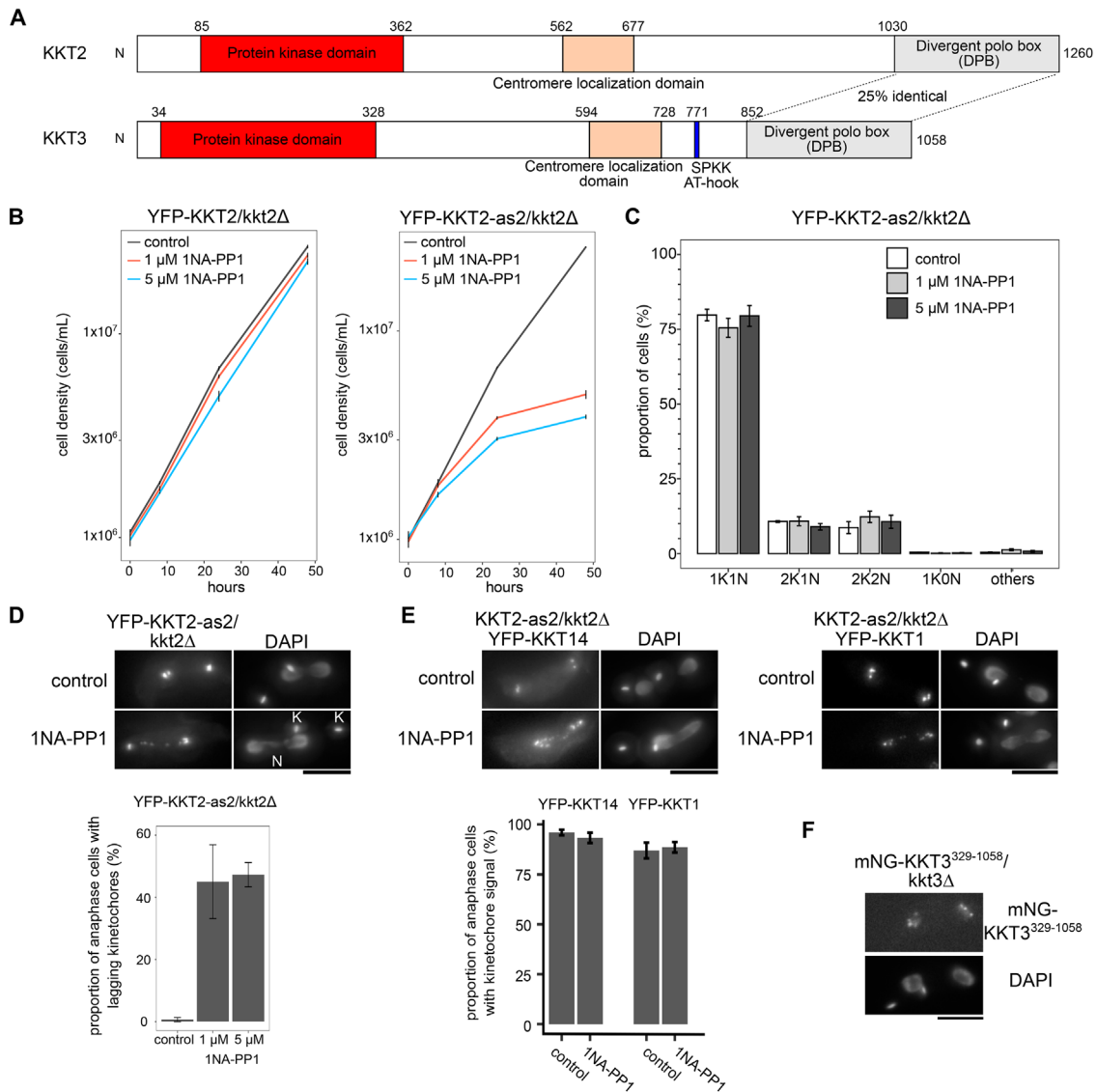


**FIGURE 1:** Kinase activity of KKT2 is essential for accurate chromosome segregation. (A) Schematics of *T. brucei* KKT2 and KKT3, highlighting the N-terminal unique kinase domain, the centromere localization domain in the middle, and C-terminal divergent polo boxes, as well as the SPKK and AT-hook DNA-binding motifs in KKT3. (B) Procytic cells that have a wild-type KKT2 copy are not sensitive to 1NA-PP1 (Left), while cells that have a KKT2-as2<sup>M161A</sup> analogue-sensitive allele impair cell growth upon addition of 1 μM or 5 μM 1NA-PP1 (Right). Control is DMSO-treated cells (0.05%). Error bars show SEM ( $n = 3$ ). Cell lines: BAP963 and BAP2269. (C) Cell cycle counts after 1NA-PP1 treatment for 8 h, showing no significant difference in the cell cycle profile. Error bars show SEM ( $n = 3$ , >240 cells each). Cell line: BAP2269. (D) Inhibition of KKT2 kinase activity causes chromosome segregation defects. Images of lagging kinetochores (Top) and quantification of anaphase cells with lagging kinetochores (Bottom) are shown. KKT2 analogue-sensitive cells were treated with 1 μM 1NA-PP1, 5 μM 1NA-PP1, or 0.05% DMSO for 8 h and fixed for microscopy. Cells treated with 1NA-PP1 have significantly more lagging kinetochores than untreated control ( $p$ -value < 0.0001, Fisher's exact test for count data [control vs 1 μM] and [control vs 5 μM]). Error bars show SEM ( $n = 3$ , >42 anaphase cells each). Cell line: BAP2269. (E) Kinetochores localization of KKT14 and KKT1 is not affected by inhibition of KKT2 kinase activity. (Top) KKT2 analogue-sensitive cells expressing YFP-KKT14 (Left) or YFP-KKT1 (Right) were treated with 5 μM 1NA-PP1 or 0.05% DMSO for 8 h and fixed for microscopy. (Bottom) Quantification of anaphase cells that had YFP dots, showing no significant difference in kinetochores localization of KKT14 and KKT1 upon inhibition of KKT2 kinase activity ( $p$ -value > 0.05,  $n = 3$ , >70 cells each). Error bars show SEM. Cell lines: BAP806 and BAP839. (F) Procytic cells can survive without the KKT3 kinase domain. Cells expressing mNeonGreen-KKT3<sup>329-1058</sup> as the sole copy of KKT3 were fixed, showing normal kinetochores localization. Cell line: BAP1014. Bars = 5 μm.

found the KKT8 complex that consists of KKT8/9/11/12 proteins (Ishii and Akiyoshi, 2020) as an *in vitro* target, where KKT2 phosphorylated KKT8 (and KKT12 to a lesser extent), and KKT3 phosphorylated KKT12 (and KKT8 to a lesser extent; Figure 2, A and B).

The kinase domain of KKT2 also phosphorylated KKT8 (Figure 2B), albeit less efficiently than the full-length protein. These results suggest that KKT2 and KKT3 kinase domains have distinct substrate specificities.

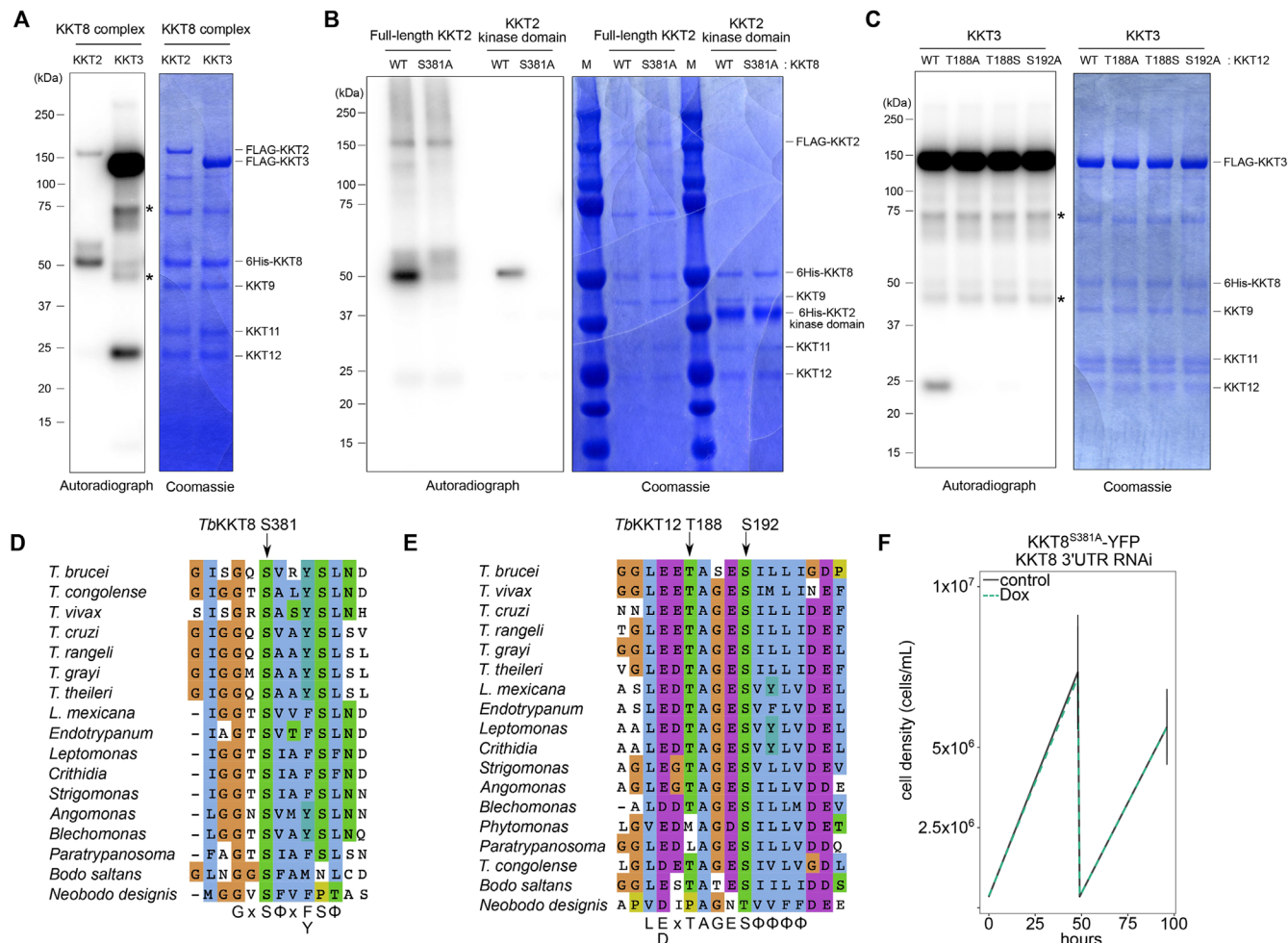


**FIGURE 2:** KKT2 phosphorylates KKT8, and KKT3 phosphorylates KKT12. (A) KKT2 phosphorylates KKT8 of the KKT8 complex, while KKT3 phosphorylates KKT12 in vitro. In vitro kinase assay was performed using the recombinant KKT8 complex with KKT2 or KKT3. The left panel shows phosphorylation detected by autoradiography, and the right panel shows the Coomassie Brilliant Blue staining. Asterisks indicate KKT3 degradation products. (B) KKT2 phosphorylates S381 of KKT8. In vitro kinase assay was performed on the KKT8 complex that has mutation in KKT8 S381A using full-length KKT2 or just the kinase domain. (C) Phosphorylation of KKT12 by KKT3 is abolished when T188 or S192 is mutated. Asterisks indicate KKT3 degradation products. (D) KKT8 S381 and the surrounding residues are well conserved among kinetoplastids. The putative phosphorylation motif of KKT2 is G-x-S\*-Φ-x-F/Y-S-Φ, where S\* gets phosphorylated and Φ represents hydrophobic residues. Note that the -2 position is Gly. (E) KKT12 T188, S192, and surrounding residues are well conserved among kinetoplastids. The putative phosphorylation motif of KKT3 is L-E/D-x-T-A-G-E-S-Φ-Φ-Φ-Φ, where either T or S (or both) gets phosphorylated. (F) KKT8<sup>S381A</sup> mutant is functional. Growth curve of KKT8<sup>S381A</sup>-YFP with KKT8 3'UTR RNAi is shown. RNAi was induced with 1 μg/ml doxycycline to deplete the wild-type allele of KKT8. Control is an uninduced cell culture (n = 3). Cell line: BAP1274.

By mutating conserved serine/threonine residues in these substrates, we identified S381 as the major site in KKT8 targeted by KKT2 (Figure 2B), while phosphorylation of KKT12 by KKT3 was significantly reduced when either T188 or S192 was mutated (T188A, T188S, and S192A) (Figure 2C). It is possible that S192 is the major phosphorylation site and that T188 is required for efficient phosphorylation of S192. An alternative possibility is that T188 is the major phosphorylation site and S192 is required for efficient phosphorylation of T188. These sites and surrounding residues are highly conserved among kinetoplastids (Figure 2, D and E; Supplemental Figures S2 and S3). It is noteworthy that the -2 position (residue 379 in KKT8) is glycine (Figure 2D), which is not commonly found in the consensus phosphorylation motif of protein kinases (Hutti et al., 2004). Interestingly, our previous work showed that the BRCT do-

main of KKT4 binds the KKT8 peptide and that phosphorylation of S381 increased the affinity (Ludzia et al., 2021). These results raise the possibility that KKT2 may regulate the KKT4 BRCT domain (of unknown function) through phosphorylation of KKT8. To examine the importance of this phosphorylation event, we performed a rescue experiment with the KKT8<sup>S381A</sup> mutant in trypanosomes. Using a previously established RNAi construct targeting its 3'UTR to deplete endogenous KKT8 (which caused a severe growth defect by day 2 postinduction; Marciàno et al., 2021) in a strain expressing KKT8<sup>S381A</sup>-YFP, we found that the KKT8<sup>S381A</sup> mutant supported cell growth (Figure 2F). Because inhibition of the KKT2 kinase activity causes growth defects (Figure 1B), this result means that KKT2 has additional targets to promote accurate chromosome segregation. More work is needed to identify such substrates.

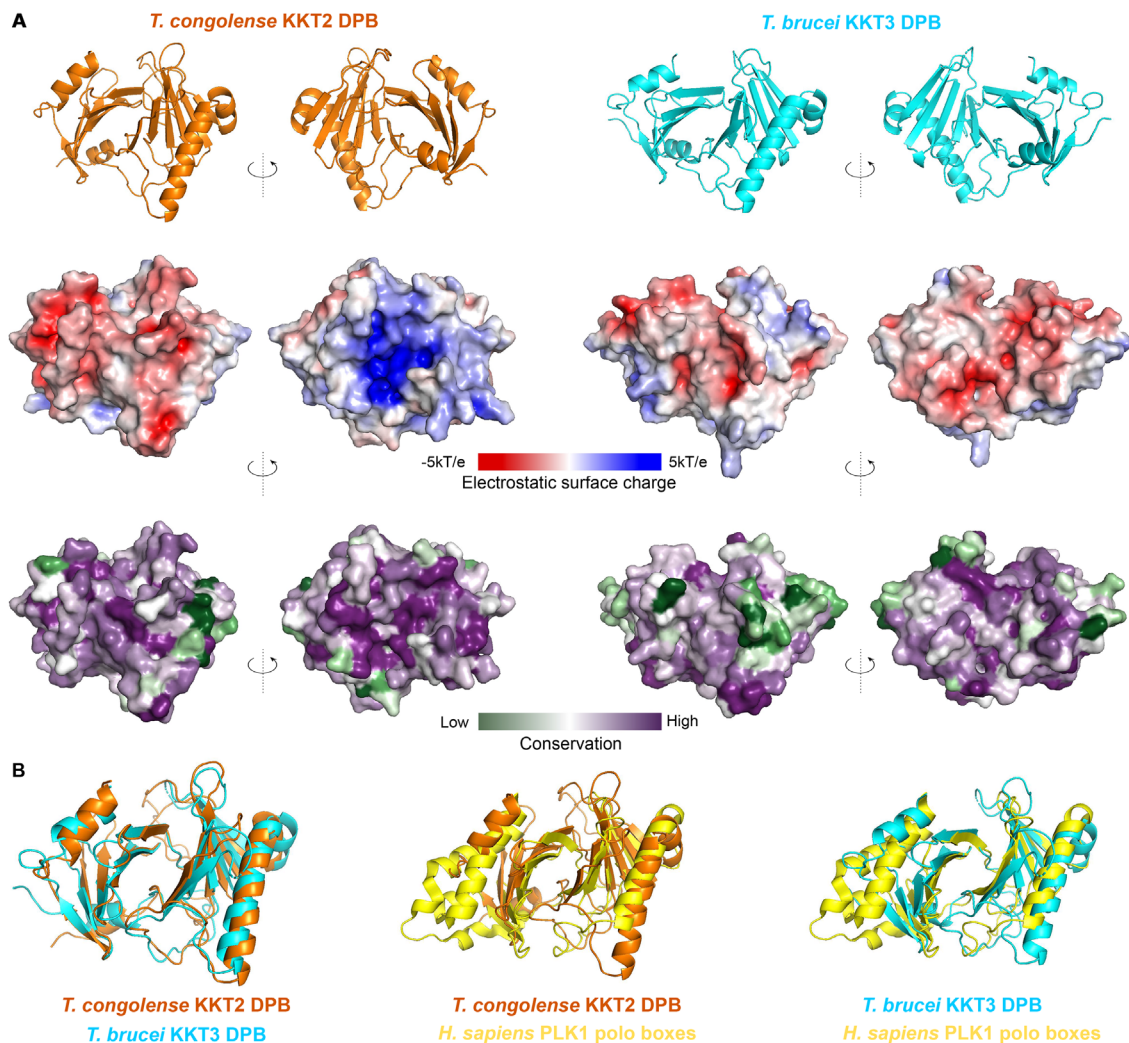


**FIGURE 3:** Crystal structures of KKT2 DPB and KKT3 DPB reveal differences. (A) Cartoon representation of the *T. congolense* KKT2 DPB (orange, left, PDB: 8A0J) and *T. brucei* KKT3 DPB (cyan, right, PDB: 8A0K), together with electrostatic surface potential and conservation of surface residues. Electrostatic surface potential of the DPBs was generated by the Adaptive Poisson–Boltzmann Solver (APBS) software (Jurrus *et al.*, 2018). Conservation of surface residues was mapped based on sequence conservation using the ConSurf server (Ashkenazy *et al.*, 2016). (B) Overlay of *T. congolense* KKT2 DPB and *T. brucei* KKT3 DPB (Left), *T. congolense* KKT2 DPB and human PLK1 polo boxes (Middle), and *T. brucei* KKT3 DPB and human PLK1 polo boxes (Right). The structure of human PLK1 polo boxes is from (Qian *et al.*, 2015; PDB: 4X9R). These structures were aligned using the “alignment” function in PyMOL.

### Crystal structures of KKT2 DPB and KKT3 DPB reveal different surface charge distributions

We next characterized the C-terminal domain of KKT2 and KKT3, which has limited sequence similarities to polo boxes of PLK1 (Nerusheva and Akiyoshi, 2016). To gain insights into the function of these divergent polo boxes, we determined their high-resolution structures by X-ray crystallography. We obtained crystals of *T. congolense* KKT2<sup>1030–1265</sup> (61.6% identical to *T. brucei* KKT2<sup>1024–1260</sup>) and determined its structure at 2.2 Å using molecular replacement with an AlphaFold2-predicted model of *T. congolense* KKT2 DPB as a search template, while the crystal structure of *T. brucei* KKT3 DPB was determined to 2.9 Å resolution using molecular replacement with a selenomethionine-derivatized crystal model (Figure 3A and Table 1). As expected from our previous sequence analysis (Nerusheva and Akiyoshi, 2016), structural homology searches using the DALI server (Holm, 2020) confirmed polo boxes of PLK1 as the closest structural homolog of KKT2/3 DPB (root-mean-square deviation

[RMSD] between *T. congolense* KKT2 DPB and human PLK1: 6.3 Å across 109 C $\alpha$ ; RMSD between *T. brucei* KKT3 DPB vs human PLK1: 4.4 Å across 112 C $\alpha$ ; Figure 3B and Supplemental Table S2). However, some key residues involved in the phosphopeptide recognition are missing in KKT2/3 DPB, as previously noted from their sequence analysis (Elia *et al.*, 2003; Nerusheva and Akiyoshi, 2016; Supplemental Figure S4), suggesting either that KKT2/3 DPB is not a phosphorylation-dependent protein–protein interaction domain or that KKT2/3 DPB interacts with phosphorylated proteins in a distinct manner.

Although KKT2 DPB and KKT3 DPB have highly similar backbones (RMSD: 2.2 Å across 129 C $\alpha$ ; Figure 3B), they have distinct patterns of surface charge and conservation (Figure 3A; Supplemental Figure S5, A and B). One notable difference is that KKT2 DPB has positively charged patches (Figure 3A and Supplemental Figure S5A). In addition, KKT2 DPB has a loop that is highly conserved among KKT2 homologues and is found even in early branching

	<i>T. congolense</i> KKT2 <sup>1030–1265</sup>	SeMet <i>T. brucei</i> KKT3 <sup>847–1058</sup>	Native <i>T. brucei</i> KKT3 <sup>847–1058</sup>
Data collection			
Beamline	Diamond Light Source I03	Diamond Light Source I04	Diamond Light Source I24
Wavelength (Å)	0.9763	0.9794	1.0072
Space group (Z)	<i>P</i> 1 2 <sub>1</sub> 1	<i>P</i> 1	<i>P</i> 1
Unit cell	48.70Å 57.13Å 83.67Å 90° 97.87° 90°	45.06Å 101.14Å 102.53Å 93.39° 94.85° 98.15°	45Å 52.49Å 102.15Å 84.11° 84.42° 73.25°
Resolution range (Å)	47.04–2.20 (2.28–2.20)	68.88–2.13 (2.17–2.13)	50.68–2.92 (2.97–2.92)
Unique reflections	23316 (2303)	96388 (4664)	19067 (926)
Completeness (%)	95.80 (100)	97.34 (94.59)	99 (98.20)
Multiplicity	6.8 (6.3)	3.4 (3.4)	3.4 (3.4)
<i>I</i> / $\sigma$ <i>I</i>	12.3 (0.7)	5.6 (0.3)	5.1 (1.4)
<i>R</i> <sub>meas</sub>	0.098 (2.714)	0.111 (1.279)	0.183 (1.249)
CC <sub>1/2</sub>	1.0 (0.4)	0.97 (0.45)	1.0 (0.54)
Wilson <i>B</i> -factor (Å <sup>2</sup> )	32.68	40.29	63.19
Refinement			
No. reflections	23299 (2300)		18988 (383)
<i>R</i> <sub>work</sub>	0.19 (0.28)		0.25 (0.38)
<i>R</i> <sub>free</sub>	0.24 (0.31)		0.27 (0.42)
Number of atoms	3674		6254
Protein	3489		6169
Ligands	0		34
Solvent	185		51
RMS bonds (Å)	0.007		0.008
RMS angles (°)	0.93		1.04
Ramachandran favored (%)	96.10		93.65
Ramachandran allowed (%)	3.90		5.72
Ramachandran outliers (%)	2.11		0.64
Average <i>B</i> -factor (Å <sup>2</sup> )	40.97		81.64

Note: Statistics for the highest-resolution shell are shown in parentheses.

**TABLE 1:** Data collection and refinement statistics.

prokinetoplastids (Supplemental Figure S5, C and D). These differences raise the possibility that KKT2 DPB and KKT3 DPB have distinct functions.

### KKT3 DPB is essential for cell proliferation and can recruit KKT2 in trypanosomes

To examine the functional importance of the divergent polo boxes of KKT2 and KKT3 for cell viability, we aimed to perform rescue experiments in trypanosomes using DPB mutants. Unfortunately, we could not analyze point mutants of KKT2/3 because they all had low-protein level problems. Instead, we managed to obtain a deletion mutant that lacked KKT3 DPB (KKT3<sup>ADPB</sup>-YFP). Using a previously established RNAi construct targeting 3'UTR of KKT3 to deplete the endogenous protein (Marcianò *et al.*, 2021), we found that KKT3<sup>ADPB</sup>-YFP failed to support cell growth when the remaining wild-type KKT3 protein was depleted by RNAi (Figure 4A). This result shows that KKT3 DPB is essential for the survival of procyclic trypanosome cells. We could not perform a similar experiment for KKT2<sup>ADPB</sup> due to a low-protein level problem.

We next aimed to reveal the function of KKT3 DPB. Our previous work showed that ectopically expressed KKT3 DPB copurified with several kinetochore proteins including KKT2, KKT8, KKT7, and KKT1 (Marcianò *et al.*, 2021). Using the LacO–LacI system (Ishii and Akiyoshi, 2020), we found that the GFP–KKT3 DPB–LacI fusion protein was able to recruit tdTomato–KKT2 to an ectopic locus (Figure 4B). This recruitment was abolished in the W863A mutant, which is expected to affect the structural integrity of the KKT3 DPB protein (Figure 4B). These results show that KKT3 DPB is a protein–protein interaction domain that binds KKT2 either directly or indirectly.

### KKT2 DPB directly interacts with the C-terminal part of KKT1

Although KKT2 DPB has sequence similarity to KKT3 DPB (25% identical), it remained unclear whether they have the same or distinct interaction partners. Indeed, our finding that the surface charges are quite different between these two proteins raised the possibility that they have distinct interaction partners. When expressed and immunoprecipitated from trypanosomes, KKT2 DPB copurified with KKT1, KKT6, KKT7 and KKT8, which was abolished

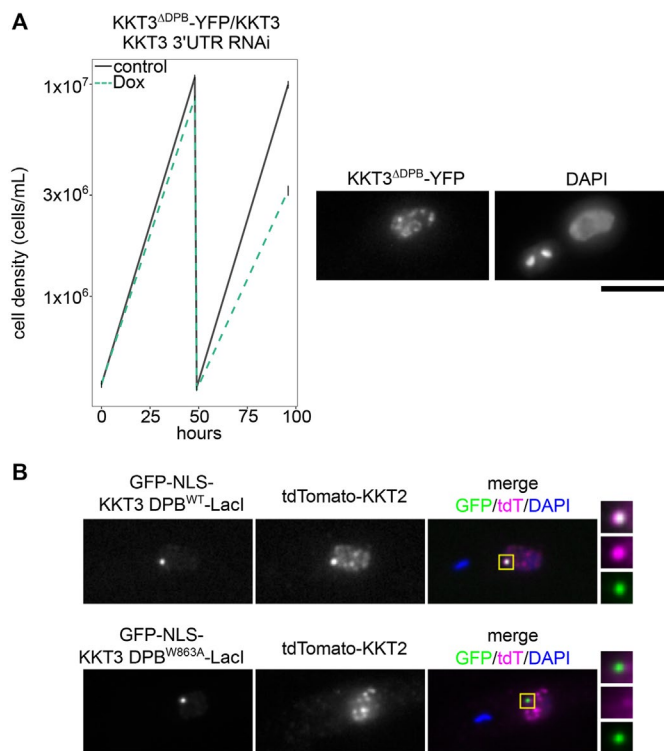


**FIGURE 4:** KKT3 DPB can recruit KKT2 to an ectopic locus. (A) KKT3<sup>1-851</sup>-YFP that lacks the DPB cannot support cell growth. Growth curve of KKT3<sup>1-851</sup>-YFP with KKT3 3'UTR RNAi is shown. RNAi was induced with 1 μg/ml doxycycline to deplete the untagged KKT3 allele. Control is an uninduced cell culture ( $n = 3$ ). Cell line: BAP2157. (B) KKT3 DPB, but not its W863A mutant, can recruit KKT2 to a noncentromeric locus in trypanosomes. Expression of GFP fusion proteins was induced in cells expressing tdTomato-KKT2 with 10 ng/mL doxycycline for 1 day. Out of 10 cells that had tdTomato signal with a clear LacI dot, recruitment of KKT2 (based on enriched tdTomato-KKT2 signal at the LacI dot position) was observed in 10 cells for wild-type KKT3 DPB or 0 cell for the W863A mutant. Cell lines: BAP2101, BAP2163. Bars = 5 μm.

when W1048 was mutated (Marcianò *et al.*, 2021). Using the LacO–LacI tethering assay, we found that KKT2 DPB can recruit KKT1 to an ectopic locus in trypanosome cells, which was abolished in the W1048A mutant (Figure 5A). Based on AlphaFold2-based structure predictions, the N-terminal part of KKT1 (1–989) is predicted to contain divergent HEAT repeats, while its C-terminal part (990–1594) is predicted to be largely disordered (Jumper *et al.*, 2021; Wheeler, 2021; Mirdita *et al.*, 2022; Varadi *et al.*, 2022). While characterizing the KKT1 protein, we found that KKT2 was detected in the immunoprecipitates of KKT1C, but not KKT1N (Figure 5B and Supplemental Table S3). Furthermore, our tethering assay showed that KKT1C was able to recruit KKT2 in trypanosome cells (Figure 5C). These results prompted us to test whether KKT2 DPB directly interacts with the C-terminal part of the KKT1 protein. Using recombinant proteins, we found that KKT2 DPB comigrated with KKT1C<sup>990-1594</sup> in size-exclusion chromatography, which separates macromolecules based on their size and shape (Figure 5D). Interestingly, KKT1C eluted later in the presence of KKT2 DPB than KKT1C itself, suggesting that KKT1C, which is predicted to be largely disordered, may adopt a more compacted structure when it is bound to KKT2 DPB. Chemical cross-linking mass spectrometry assays identified a number of cross-links between the two proteins (Figure 5E and Supplemental Table

S4). Taken together, these results establish that KKT2 DPB interacts directly with KKT1. In contrast, no apparent shift was observed for KKT3 DPB when mixed with KKT1C, suggesting that these proteins do not interact, at least under the conditions used in our assay (Figure 5D).

### KKT1 forms a complex with KKT6

To better understand the mechanism of kinetochore assembly, we next aimed to identify interaction partners for KKT1. In the immunoprecipitates of KKT1, many kinetochore proteins were identified, specifically KKT2–13 (Akiyoshi and Gull, 2014). KKT5, KKT6, and KKT7 have a localization pattern similar to that of KKT1, so we tested whether they directly bind KKT1. By coexpressing FLAG-tagged KKT1 with untagged KKT5, KKT6, and KKT7 (and untagged KKT2, which turned out to be mostly insoluble; Supplemental Figure S1B), we found that KKT6 (and KKT7 to a lesser extent) co-purified with FLAG-KKT1 (Supplemental Figure S1C). To confirm this result, we next coexpressed only FLAG-KKT6 and KKT1 and found that these proteins copurified (Figure 6A). Cross-linking mass spectrometry identified many cross-links between KKT1 and KKT6 (Figure 6B and Supplemental Table S4). We therefore identified KKT6 as a direct interaction partner for KKT1.

### DISCUSSION

Growing evidence points to the importance of KKT2 and KKT3 in the kinetoplastid kinetochores. These proteins have DNA-binding motifs, localize constitutively at kinetochores, and contribute to the recruitment of multiple kinetochore proteins, suggesting that KKT2 and KKT3 sit at the base of kinetoplastid kinetochores (Marcianò *et al.*, 2021). These proteins share common ancestry with polo-like kinases and have an N-terminal protein kinase domain and C-terminal divergent polo boxes (Nerusheva and Akiyoshi, 2016). KKT2 and KKT3 additionally have a unique central domain that promotes centromere localization of these proteins (Marcianò *et al.*, 2021). Homologues of KKT2/3 are found in essentially all sequenced kinetoplastids, although early-branching prokinetoplastids have KKT2-like proteins, rather than KKT3 (Butenko *et al.*, 2020). We therefore speculated that ancestral kinetoplastids had only KKT2-like proteins that performed all necessary functions and that KKT3 in trypanosomatids represents a gene duplication product that became specialized in more efficient centromere localization (Marcianò *et al.*, 2021). Our findings in this study highlight the difference between KKT2 and KKT3. The kinase activity of KKT2 is essential for accurate chromosome segregation, while that of KKT3 is dispensable for cell growth in the procyclic form *T. brucei*. Furthermore, KKT2 phosphorylates KKT8 of the KKT8 complex (which consists of KKT8/9/11/12), while KKT3 phosphorylates KKT12. Given that the KKT8 complex promotes kinetochore localization of the KKT10/19<sup>CLK</sup> kinases (Ishii and Akiyoshi, 2020), these phosphorylation events might regulate the activity of KKT10/19.

Another difference between KKT2 and KKT3 is their interaction partner. Our analysis identified the C-terminal domain of KKT1 as the direct interaction partner for KKT2 DPB, but not for KKT3 DPB. However, it is important to mention that kinetochore localization of KKT1 was not significantly affected when KKT2 was depleted by RNAi but was affected when both KKT2 and KKT3 were depleted (Marcianò *et al.*, 2021). These results imply redundancy in kinetochore recruitment of KKT1. It will be important to obtain a comprehensive interaction map of kinetoplastid kinetochore proteins. It will also be important to understand the molecular basis of the KKT2/KKT1 interaction in the future. Analysis of the cross-linking mass spectrometry result (using the zero-length cross-linker EDC) for the

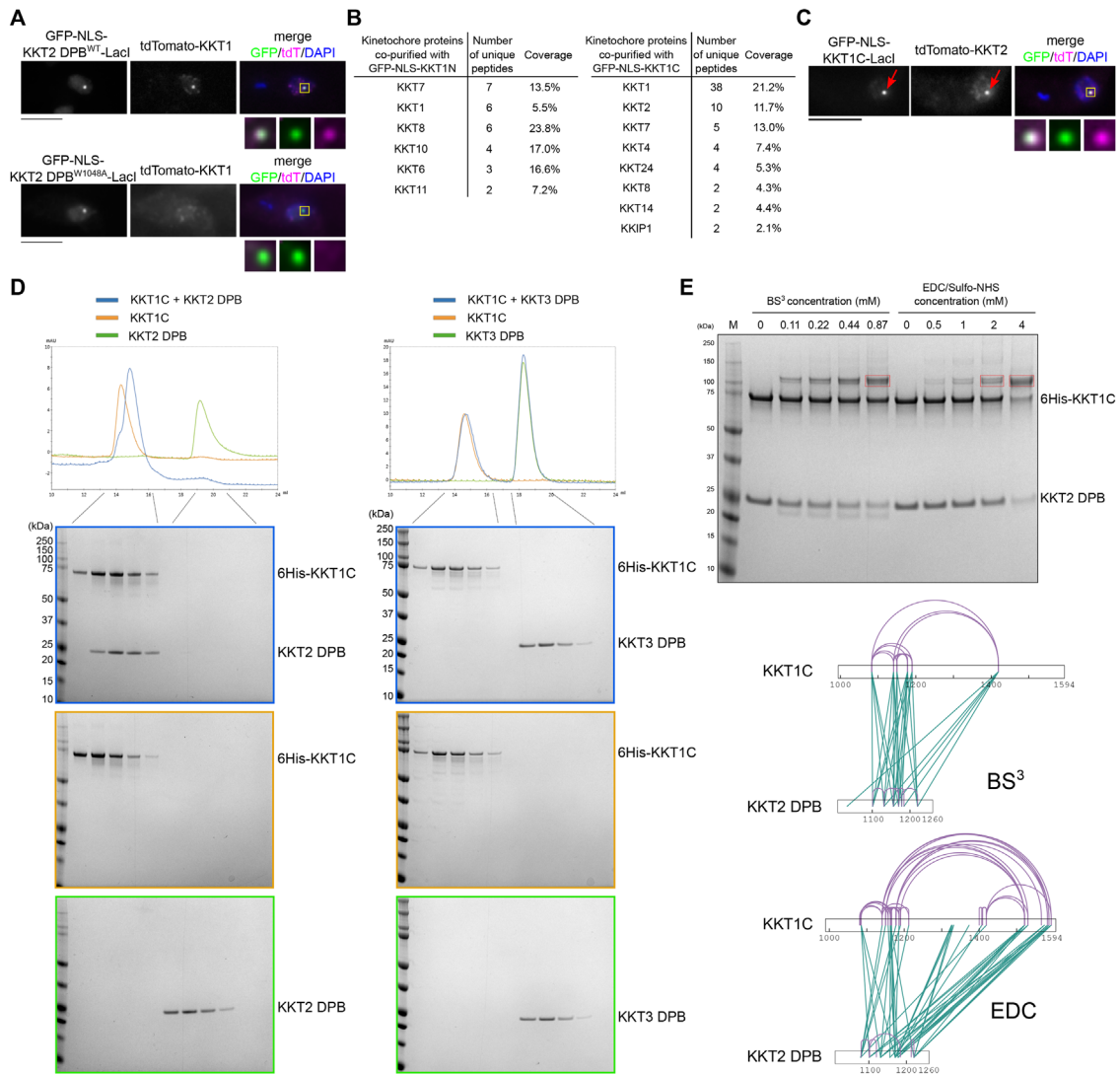


**FIGURE 5:** KKT2 DPB interacts directly with KKT1. (A) KKT2 DPB, but not its W1048A mutant, is sufficient to recruit KKT1 to a noncentromeric locus in trypanosomes. Out of 10 cells that had tdTomato signal with a clear Lacl dot, recruitment of KKT1 (based on enriched tdTomato-KKT1 signal at the Lacl dot position) was observed in nine cells for wild-type KKT2 DPB or 0 cell for the W1048A mutant. Cell lines: BAP1233, BAP2162. (B) Ectopically expressed GFP-NLS-KKT1C<sup>990-1594</sup>, but not GFP-NLS-KKT1N<sup>2-989</sup>, copurifies with KKT2. See Supplemental Table S3 for all proteins identified by mass spectrometry. Cell lines: BAP272, BAP273. (C) KKT1C<sup>990-1594</sup> can recruit KKT2 to an ectopic locus in cells. Cell line: BAP2330. Out of 10 cells that had tdTomato signal with a clear Lacl dot, recruitment of KKT2 (based on enriched tdTomato-KKT2 signal at the Lacl dot position) was observed in 10 cells. For A–C, expression of GFP fusion proteins was induced with 10 ng/mL doxycycline for 1 day. Bars = 5  $\mu$ m. (D) KKT2 DPB<sup>1024-1260</sup>, not KKT3 DPB<sup>832-1058</sup>, forms a complex with KKT1C<sup>990-1594</sup>. Recombinant proteins were mixed on ice for 30 min, followed by analytical size-exclusion chromatography on a Superose 6 10/300 column. (E) Cross-linking mass spectrometry of the KKT2 DPB/KKT1C complex using BS<sup>3</sup> or EDC/Sulfo-NHS, showing extensive cross-links between the two proteins. The bands highlighted in red boxes were digested with trypsin and analyzed by mass spectrometry. Green lines indicate intermolecular cross-links and purple lines indicate intramolecular cross-links. See Supplemental Table S4 for all cross-links identified by mass spectrometry.

AlphaFold2-predicted structure of *T. brucei* KKT2 DPB implies the presence of widespread contacts between KKT2 DPB and KKT1C. It is worth mentioning that it represents the first direct protein–protein interaction identified between a constitutive kinetochore protein (KKT2) and a transient kinetochore protein that localizes from S phase onward (KKT1). How is the recruitment of KKT1 onto KKT2 regulated during cell cycle? Although cyclin-dependent kinases play crucial roles in cell cycle-regulated recruitment of kinetochore proteins in other eukaryotes (Gascoigne and Cheeseman, 2013), our

previous study found that kinetochore localization of KKT1 or other examined proteins was not affected by depletion of a mitotic cyclin in *T. brucei* (Hayashi and Akiyoshi, 2018). Based on the observation that the transcript of KKT1 is highly up-regulated in the S phase, it might be that KKT1 proteins are simply absent in G1 (Archer *et al.*, 2011). Consistent with this possibility, the identified interaction between KKT2 DPB and KKT1C likely does not rely on phosphorylation because these proteins were expressed and purified from *E. coli*. Interestingly, not only KKT2/3 DPB but also polo boxes of the

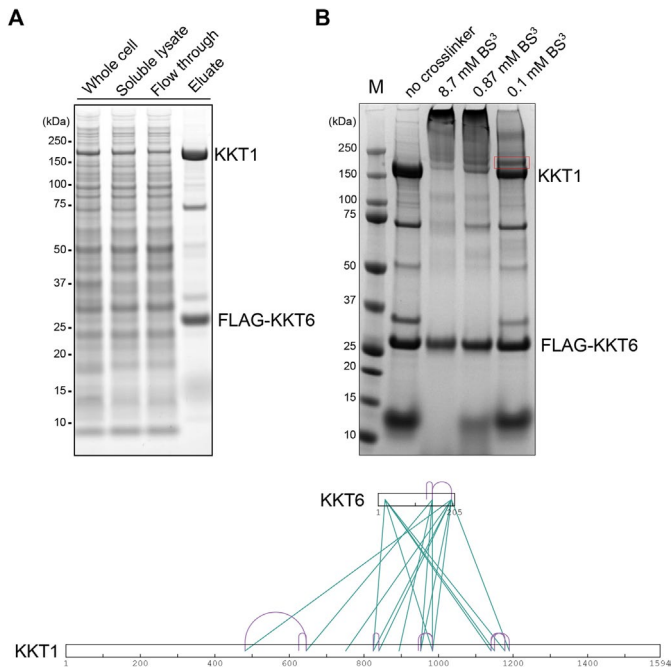


**FIGURE 6: KKT1 interacts with KKT6.** (A) KKT1 copurifies with FLAG-KKT6. These proteins were coexpressed and purified from insect cells with anti-FLAG antibodies. (B) Cross-linking mass spectrometry of the KKT1/KKT6 complex using BS<sup>3</sup>. The band highlighted in the red box was digested with trypsin and analyzed by mass spectrometry. Green lines indicate intermolecular cross-links and purple lines indicate intramolecular cross-links. See Supplemental Table S4 for all cross-links identified by mass spectrometry.

PLK1 homolog in *T. brucei* (called TbPLK), which plays important roles in regulating cytoplasmic events such as the duplication of basal bodies and Golgi as well as cytokinesis, lack key residues involved in phosphopeptide binding in human PLK1 (Yu et al., 2012; McAllaster et al., 2015). Sequence analysis of PLK1 in *Naegleria* also suggests that its polo boxes are unlikely to act as a phosphopeptide binding domain (Nerusheva and Akiyoshi, 2016). We speculate that the last common ancestor of PLK1 might have been a phosphorylation-independent protein-protein interaction domain.

It has been shown that kinetoplastid kinetochores proteins are unique therapeutic targets against not only *T. brucei* but also *Leishmania* and *T. cruzi* (Nishino et al., 2013; Saldivia et al., 2020). Further understanding of the molecular function and structure of the unique kinetoplastid kinetochore proteins could facilitate the development of specific and efficient drugs against neglected tropical diseases caused by kinetoplastid parasites.

## MATERIALS AND METHODS

### Primers, plasmids, bacmids, and synthetic DNA

All primers, plasmids, bacmids, and synthetic DNA used in this study are listed in Supplemental Table S1. Their source or construction details are explained in Supplemental Table S1. All constructs were sequence verified.

### Trypanosome cells

All trypanosome cell lines used in this study were derived from *T. brucei* SmOxP927 procyclic form cells (TREU 927/4 expressing T7 RNA polymerase and the tetracycline repressor to allow inducible expression; Poon et al., 2012) and are listed in Supplemental Table S1. Cells were grown at 28°C in SDM-79 medium supplemented with

10% (vol/vol) heat-inactivated fetal calf serum, 7.5 µg/ml hemin (Brun and Schönberger, 1979), and appropriate drugs. Endogenous YFP tagging was performed using the pEnT5-Y vector (Kelly et al., 2007) or a PCR-based method (Dean et al., 2015). Endogenous tdTomato tagging was performed using pBA148 (Akiyoshi and Gull, 2014) and its derivatives. LacO–LacI tethering experiments were performed as described previously using the LacO array inserted at the rDNA locus (Landeira and Navarro, 2007; Ishii and Akiyoshi, 2020). Inducible expression of GFP-NLS fusion and GFP-NLS-LacI fusion proteins was carried out using pBA310 (Nerusheva and Akiyoshi, 2016) and pBA795 (Ishii and Akiyoshi, 2020), respectively. Cell growth was monitored using a CASY cell counter (Roche). Expression of GFP fusion proteins and RNAi was induced with doxycycline at a final concentration of 10 ng/mL and 1 µg/ml, respectively. One allele of KKT2 or KKT3 was deleted by a PCR-based method using neomycin cassettes and primers listed in Supplemental Table S1 (Merritt and Stuart, 2013; Ishii and Akiyoshi, 2020). To make a strain that lacks the KKT3 kinase domain, an N-terminal mNeonGreen tag was inserted between the kinase domain and the rest of the KKT3 coding sequence. Similarly, a C-terminal YFP tag was inserted just before the DPB of KKT3 to delete its DPB. Analog sensitive alleles or kinase dead mutants of KKT2/3 were made using endogenous tagging plasmids that contained appropriate mutations. Gatekeeper residues of KKT2 (M161) and KKT3 (M109) were determined by multiple sequence alignment with other protein kinases that have known gatekeeper residues. The cell line that has *kkt3Δ/KKT3-as1* (M109G) grew normally in the presence of 2.5 µM of 1NA-PP1, 1NM-PP1, or 3MB-PP1 (unpublished data). To make deletion or mutant cell lines, transfected cells were selected with appropriate drugs and cloned by dispensing dilutions into 96-well plates and screened by PCR and/or DNA sequencing. All plasmids were linearized by *NotI* and transfected into trypanosomes by electroporation. Transfected cells were selected by the addition of 30 µg/ml G418 (Sigma), 25 µg/ml hygromycin (Sigma), 5 µg/ml phleomycin (Sigma), or 10 µg/ml blasticidin S (Insight biotechnology).

### Fluorescence microscopy

Cells were fixed with 4% paraformaldehyde for 5 min as described previously (Nerusheva and Akiyoshi, 2016), and images were captured at room temperature on a DeltaVision fluorescence microscope (Applied Precision) installed with softWoRx v.5.5 housed in the Oxford Micron facility essentially as described using a CoolSNAP HQ camera with 60x objective lenses (1.42 NA) or on a Zeiss Axioimager.Z2 microscope (Zeiss) installed with ZEN using a Hamamatsu ORCA-Flash4.0 camera with 63x objective lenses (1.40 NA). Typically, ~20 optical slices spaced 0.2 or 0.24 µm apart were collected. Images were processed in ImageJ/Fiji (Schneider et al., 2012). Maximum-intensity projection images were generated by Fiji software (Schneider et al., 2012). Figures were made using Inkscape (The Inkscape Team).

### Multiple sequence alignment

Protein sequences and accession numbers for KKT2, KKT3, KKT8, and KKT12 homologues used this study were retrieved from the TriTryp database (Aslett et al., 2010), UniProt (UniProt Consortium, 2019), or published studies (Tanifuji et al., 2017; Butenko et al., 2020; Tikhonenkov et al., 2021). Searches for homologous proteins were done using BLAST in the TriTryp database (Aslett et al., 2010). Searches for KKT2 and KKT3 homologues in Prokinetoplastina and Bodonida were done using hmmsearch on predicted proteome using manually prepared hmm profiles (HMMER version 3.0; Eddy, 1998). Multiple sequence alignment was performed

with MAFFT (L-INS-i method, version 7; Katoh et al., 2019) and visualized with the Clustalx coloring scheme in Jalview (version 2.11; Waterhouse et al., 2009).

### Expression and purification of *Trypanosoma congolense* KKT2<sup>1030-1265</sup>

*Trypanosoma congolense* KKT2<sup>1030-1265</sup> used in this study was amplified from a synthesized gene fragment (BAG170) using BA3457 and BA3458 primers and cloned into the pRSFDuet-1 vector using NEBuilder Assembly 2x Master Mix (New England Biolabs) to make pBA2558 (*T. congolense* KKT2<sup>1030-1265</sup> with an N-terminal tobacco etch virus [TEV]-cleavable hexahistidine [6His] tag). *Escherichia coli* BL21(DE3) cells were transformed with ~100 ng of plasmid DNA (pBA2558) and inoculated into 50 ml of 2xTY medium containing 50 µg/ml kanamycin and grown overnight at 37°C. In the next morning, each of the 6 L of 2xTY medium with 50 µg/ml kanamycin was inoculated with 5 ml of the overnight culture and grown at 37°C with shaking (200 rpm) until the OD<sub>600</sub> reached ~0.8. Protein expression was induced with 0.2 mM IPTG for ~16 h at 20°C.

Cells were spun down at 3400 × g at 4°C and resuspended in 200 ml of lysis buffer (50 mM sodium phosphate, pH 7.5, 500 mM NaCl, and 10% glycerol) supplemented with protease inhibitors (20 µg/ml leupeptin, 20 µg/ml pepstatin, 20 µg/ml E-64, and 0.4 mM PMSF), benzonase nuclease (500 unit/L), and 0.5 mM TCEP. All subsequent steps were performed at 4°C. Bacterial cultures were mechanically disrupted using a French press (one passage at 20,000 psi) and the soluble fraction was separated by centrifugation at 48,000 × g for 30 min. Supernatants were loaded on 5 ml of TALON beads (Takara) preequilibrated with lysis buffer. Next, the beads were washed with ~300 ml of the lysis buffer without protease inhibitors and proteins were eluted with 50 mM sodium phosphate pH 7.5, 500 mM NaCl, 10% glycerol, 250 mM imidazole, and 0.5 mM TCEP. To cleave off the His-tag, samples were incubated with TEV protease in 1:50 wt/wt ratio overnight while being buffer-exchanged into 25 mM sodium phosphate, 250 mM NaCl, 5% glycerol, 5 mM imidazole, and 0.5 mM TCEP by dialysis. To increase the sample purity and remove the 6His tag, samples were reloaded on TALON beads preequilibrated with dialysis buffer and the flow-through was collected. Next, the sample was concentrated using 10-kD MW Amicon concentrator (Millipore) and loaded onto HiPrep Superdex 75 16/600 (GE Healthcare) columns to further purify and buffer exchange into 25 mM HEPES pH 7.5, 150 mM NaCl with 0.5 mM TCEP. Fractions containing KKT2 were pooled, concentrated to 12.6 mg/ml using a 10-kD MW Amicon concentrator (Millipore), and flash-frozen in liquid nitrogen for -80°C storage. Protein concentration was measured using absorbance at 280 nm and extinction coefficient calculated based on the protein sequence.

### Expression and purification of *Trypanosoma brucei* KKT2 DPB, KKT3 DPB<sup>832-1058</sup>, KKT1C, KKT2 kinase domain, and the KKT8 complex from *Escherichia coli*

The recombinant proteins were purified based on the protocol used for *T. congolense* KKT2<sup>1030-1265</sup> purification (see above) with the following modifications.

**KKT2 DPB<sup>1024-1260</sup> (pBA2240):** Protein expression was induced at 30°C overnight using a 24-L culture. After cell lysis with French press, Tween-20 was added to a final concentration of 0.2%. Dialysis was performed using buffer containing 25 mM HEPES, 200 mM NaCl, and 0.5 mM TCEP. Protein was then subjected to ion exchange chromatography using Resource S column with buffer A (25 mM HEPES pH 7.5, 0.5 mM TCEP) and buffer B (25 mM HEPES pH 7.5, 1 M NaCl, 0.5 mM TCEP), followed by size-exclusion chroma-

tography on HiPrep Superdex 75 16/600 (GE Healthcare) in 25 mM HEPES pH 7.5, 100 mM NaCl with 0.5 mM TCEP.

**KKT3 DPB<sup>832-1058</sup> (pBA2161):** A 6-L culture was used. Dialysis was performed using 50 mM sodium phosphate, pH 7.5, 500 mM NaCl, 10% glycerol, 5 mM imidazole, and 0.5 mM TCEP, followed by ion exchange chromatography using Resource Q column with buffer A (25 mM HEPES pH 7.5, 0.5 mM TCEP) and buffer B (25 mM HEPES pH 7.5, 1 M NaCl, 0.5 mM TCEP) and size-exclusion chromatography on HiPrep Superdex 75 16/600 (GE Healthcare) in 25 mM HEPES pH 7.5, 150 mM NaCl with 0.5 mM TCEP.

**6His-KKT1C<sup>990-1594</sup> (pBA718):** A 6-L culture was used, protein expression was induced at 37°C for 4 h, and the 6His tag was not cleaved for KKT1C. Immediately after elution from TALON beads, the protein was diluted with buffer A (25 mM HEPES pH 7.5, 0.5 mM TCEP) to a final concentration of 50 mM NaCl and further purified on ion exchange chromatography using Resource Q column with buffer A (25 mM HEPES pH 7.5, 0.5 mM TCEP) and buffer B (25 mM HEPES pH 7.5, 1 M NaCl, 0.5 mM TCEP). Size-exclusion chromatography was done on HiPrep Superdex 200 16/600 (GE Healthcare) in 25 mM HEPES pH 7.5, 150 mM NaCl with 0.5 mM TCEP.

**6His-KKT2 kinase domain (pBA318):** A 2.4-L culture of Rosetta (DE3) *E. coli* cells were grown at 16°C, and 1 ml of Talon beads were used. Eluted proteins (without TEV cleavage) were further purified on Superdex 200 16/600 (GE Healthcare) in 25 mM HEPES pH 7.5, 150 mM NaCl with 0.5 mM TCEP. Fractions that correspond to a monomer peak was collected and used for in vitro kinase assay.

**The KKT8 complex that consists of 6His-KKT8 KKT9 KKT11 KKT12 (pBA457):** A 50-ml culture of Rosetta (DE3) *E. coli* cells were grown at 16°C. Bacterial cultures were disrupted using sonication (three rounds of 40 s pulse and 1 min pause, Sonicator VCX-130 PB), the soluble fraction was separated by centrifugation at 21,000 g for 30 min, and 0.1 ml of Talon beads were used. Eluted proteins (without TEV cleavage) were used for in vitro kinase assay.

### Expression and purification of *Trypanosoma brucei* KKT3<sup>847-1058</sup>

*Trypanosoma brucei* KKT3<sup>847-1058</sup> was amplified from genomic DNA using primers BA676/BA600 and cloned into pNIC28-Bsa4 (Gileadi et al., 2008) using ligation-independent cloning to make pBA295 (*T. brucei* KKT3<sup>847-1058</sup> with an N-terminal TEV-cleavable 6His tag). Recombinant protein was expressed in Rosetta (DE3) *E. coli* cells at 20°C using 12 L of 2xTY media. L-selenomethionine-labeled *T. brucei* KKT3<sup>847-1058</sup> (SeMet *T. brucei* KKT3<sup>847-1058</sup>) recombinant protein was expressed in BL21(DE3) *E. coli* cells at 20°C using 6 L of medium base plus nutrient mix (SelenoMet medium, Molecular Dimensions). Cells were initially grown overnight in 2xTY media (100 ml) and then centrifuged and resuspended twice with 60 ml of medium base plus nutrient mix. Each flask was inoculated with 10 ml of final resuspension, grown until OD<sub>600</sub> of 0.6–0.8, and then supplemented with L-selenomethionine (65 mg per liter of media, Anagrade) and 0.2 mM IPTG.

Cells were harvested by centrifugation and resuspended in 25 ml lysis buffer (25 mM HEPES pH 7.5, 150 mM NaCl, 10 mM imidazole, and 0.5 mM TCEP for unlabeled protein or 2 mM TCEP for labeled protein) per liter of culture. Cells were mechanically disrupted using French press (one passage at 20,000 psi) and then centrifuged at 48,000 × g for 30 min at 4°C. Tagged proteins were purified from lysate using 5 ml TALON beads (Takara), washed with 150 ml lysis buffer, and eluted with 22 ml of elution buffer (25 mM HEPES pH 7.5, 150 mM NaCl, 250 mM imidazole and 0.5 mM TCEP for unlabeled protein or 2 mM TCEP for labeled protein), followed by overnight incubation with TEV protease in dialysis buffer (25 mM HEPES

pH 7.5, 150 mM NaCl, 5 mM imidazole and 0.5 mM TCEP for unlabeled protein or 2 mM TCEP for labeled protein). Finally, a 5-ml TALON beads column was used to remove the 6His tag and other contaminants from our sample. Cleaved protein was concentrated with an Amicon centrifugal filter with 10-kD cutoff (Merck) and then further purified by size-exclusion chromatography using HiPrep Superdex 75 16/600 (GE Healthcare) pre-equilibrated with 25 mM HEPES (pH 7.5), 150 mM NaCl, and 0.5 mM TCEP for unlabeled protein or 4 mM TCEP for labeled protein. Fractions containing proteins were pooled together and concentrated to 12.2 mg/ml and 18.6 mg/ml for labeled protein and stored at -80°C. Protein concentration was measured by Bradford assay.

### Expression and purification of recombinant proteins from insect cells

3FLAG-KKT1 (bacmid pBA386), 3FLAG-KKT2 (bacmid pBA388), 3FLAG-KKT3 (bacmid pBA358), FLAG-KKT6/KKT1 (bacmid pBA828), 3FLAG-KKT1/KKT2 (bacmid pBA521), or 3FLAG-KKT1/KKT2/KKT5/KKT6/KKT7 (bacmid pBA523) was expressed in insect cells using the MultiBac baculovirus expression system (Bieniossek *et al.*, 2012; Geneva Biotech) using a protocol described previously (Llauró *et al.*, 2018). Proteins were eluted in BH0.25 (25 mM HEPES, pH 7.5, 2 mM MgCl<sub>2</sub>, 0.1 mM EDTA, 0.5 mM EGTA, 10% glycerol, and 250 mM NaCl) supplemented with 0.5 mg/ml 3FLAG peptide (Sigma).

### Analytical size-exclusion chromatography

KKT2 DPB<sup>1024-1260</sup> (8 μM) and 6His-KKT1C (8 μM) were mixed for 30 min on ice. KKT3 DPB<sup>832-1058</sup> (7 μM) and 6His-KKT1C (7 μM) were mixed for 30 min on ice. All samples were in gel filtration buffer (25 mM HEPES pH 7.5, 150 mM NaCl with 0.5 mM TCEP). Analytical size-exclusion chromatography was carried out on a Superose 6 10/300 (GE Healthcare) using a gel filtration buffer on an ÄKTA pure system (GE Healthcare) at a flow rate of 0.5 ml/min at 4°C. Elution of proteins was monitored at 280 nm. Fractions of 500 μl were collected and analyzed by SDS-PAGE and Coomassie blue staining.

### Chemical cross-linking mass spectrometry

Cross-linking reactions were performed using BS<sup>3</sup> and/or EDC/Sulfo-NHS essentially as described previously (Ludzia *et al.*, 2021) using the following samples: ~2 μM of FLAG-KKT6/KKT1 in 25 mM HEPES pH 8.0, 2 mM MgCl<sub>2</sub>, 0.1 mM EDTA, 0.5 mM EGTA-KOH, 10% glycerol, 250 mM NaCl, 0.1% NP40, and 0.5 mg/ml 3FLAG peptide, or KKT2 DPB/KKT1C (taken from the analytical size-exclusion chromatography experiment) in 25 mM HEPES pH 7.5, 150 mM NaCl with 0.5 mM TCEP. The cross-linked sample for the FLAG-KKT6/KKT1 complex was analyzed in the Advanced Proteomics Facility (<https://www.proteomics.ox.ac.uk/>). The gel band corresponding to cross-linked species was cut out, followed by in-gel trypsin digestion and LC-MS/MS analysis using a QExactive Orbitrap Mass Spectrometer (Thermo) as described previously (Ludzia *et al.*, 2021). The cross-linked samples for KKT2 DPB/KKT1C complex were analyzed in the proteomics core facility at EMBL Heidelberg (<https://www.embl.org/groups/proteomics/>). The bands were subjected to in-gel digestion with trypsin (Savitski *et al.*, 2014). Peptides were extracted from the gel pieces by sonication for 15 min, followed by centrifugation and supernatant collection. A solution of 50:50 water: acetonitrile, 1% formic acid (2x the volume of the gel pieces) was added for a second extraction and the samples were again sonicated for 15 min and centrifuged and the supernatant was pooled with the first extract. The pooled supernatants were processed using speed vacuum centrifugation. The samples were dissolved in 10 μl of reconstitution

buffer (96:4 water: acetonitrile, 1% formic acid) and analyzed by LC-MS/MS. An UltiMate 3000 RSLC nano LC system (Dionex) fitted with a trapping cartridge (μ-Precolumn C18 PepMap 100, 5 μm, 300 μm i.d. × 5 mm, 100 Å) and an analytical column (nanoEase M/Z HSS T3 column 75 μm × 250 mm C18, 1.8 μm, 100 Å, Waters). Trapping was carried out with a constant flow of trapping solution (0.05% trifluoroacetic acid in water) onto the trapping column at 30 μl/min for 6 min. Subsequently, peptides were eluted via the analytical column running solvent A (0.1% formic acid in water) with a constant flow of 0.3 μl/min, with an increasing percentage of solvent B (0.1% formic acid in acetonitrile). The outlet of the analytical column was coupled directly to an Orbitrap QExactive plus Mass Spectrometer (Thermo) using the Nanospray Flex ion source in positive ion mode. The peptides were introduced into the QExactive plus via a Pico-Tip Emitter 360 μm OD × 20 μm ID; 10 μm tip (New Objective) and an applied spray voltage of 2.2 kV. The capillary temperature was set at 275°C. A full mass scan was acquired with mass range 350–1500 *m/z* in profile mode with a resolution of 70,000. The filling time was set at a maximum of 50 ms with a limitation of 3 × 10<sup>6</sup> ions. Data-dependent acquisition (DDA) was performed with the resolution of the Orbitrap set to 17,500, with a fill time of 120 ms and a limitation of 5 × 10<sup>4</sup> ions. A normalized collision energy of 30 was applied. Dynamic exclusion time of 30 s was used. The peptide match algorithm was set to “preferred” and charge exclusion to “unassigned”; charge states 1 and 2 were excluded. MS<sup>2</sup> data were acquired in centroid mode.

RAW MS files were searched by the pLink 2 software (Chen *et al.*, 2019) using a FASTA database containing KKT1–20, KKT22–25, KKIP1, KKIP5, KKIP7, AUK1, CPC1, CPC2, KIN-A, KIN-B, and alpha/beta tubulins. Search parameters were as follows: maximum number of missed cleavages = 2, fixed modification = carbamidomethyl-Cys, variable modification Oxidation-Met. Precursor tolerance was set to 10 ppm. All the identified cross-links are shown in Supplemental Table S4 (FDR 5%). Cross-links that have score <1 × 10<sup>-4</sup> are visualized in Figure 5 and Figure 6 using xiNET (Combe *et al.*, 2015). All raw mass spectrometry files and custom database files used in this study have been deposited with the ProteomeXchange Consortium via the PRIDE partner repository (Perez-Riverol *et al.*, 2019; Deutsch *et al.*, 2020) with the dataset identifier PXD034039.

### Immunoprecipitation from trypanosomes and mass spectrometry

Expression of GFP-NLS-tagged KKT1N and KKT1C in trypanosomes was induced with 10 ng/ml doxycycline for 24 h. Immunoprecipitation and mass spectrometry of these KKT1 fragments was performed with anti-GFP antibodies using a method we previously described (Ishii and Akiyoshi, 2020). Peptides were analyzed by electrospray tandem mass spectrometry over a 60-min gradient using QExactive (Thermo) at the Advanced Proteomics Facility (University of Oxford). RAW MS files were analyzed using MaxQuant version 2.0.1 (Cox and Mann, 2008) on a custom *T. brucei* proteome database that contains predicted proteins in TriTrypDB (TREU927, version 4; Aslett *et al.*, 2010) supplemented with predicted small proteins (Ericson *et al.*, 2014; Parsons *et al.*, 2015) with carbamidomethyl cysteine as a fixed modification and up to two missed cleavages allowed (protein FDR 1%). Default values were used except as follows. Oxidization (Met), phosphorylation (Ser, Thr, and Tyr), and acetylation (Lys) were searched as variable modifications. The first peptide tolerance was set to 10 ppm. Proteins identified with at least two peptides were considered as significant and shown in Supplemental Table S3.

## In vitro kinase assay

A quantity of 10  $\mu$ l of the recombinant KKT8 complex (~0.4 mg/ml in 50 mM sodium phosphate, pH 7.5, 500 mM NaCl, and 10% glycerol, and 250 mM imidazole; Ishii and Akiyoshi, 2020) was mixed with 5  $\mu$ l of recombinant kinase (3FLAG-KKT2: 0.22 mg/ml in 25 mM HEPES pH 8.0, 2 mM MgCl<sub>2</sub>, 0.1 mM EDTA, 0.5 mM EGTA-KOH, 10% glycerol, 250 mM NaCl, 0.1% NP40, and 0.5 mg/ml 3FLAG peptide; 3FLAG-KKT3: 0.5 mg/ml in 25 mM HEPES pH 8.0, 2 mM MgCl<sub>2</sub>, 0.1 mM EDTA, 0.5 mM EGTA-KOH, 10% glycerol, 250 mM NaCl, 0.1% NP40, and 0.5 mg/ml 3FLAG peptide; 6His-KKT2 kinase domain<sup>60–382</sup>: 0.4 mg/ml in 25 mM HEPES pH 7.5, 150 mM NaCl with 0.5 mM TCEP) in 1 $\times$  kinase buffer (50 mM Tris-HCl pH 7.4, 1 mM DTT, 25 mM  $\beta$ -glycerophosphate, 5 mM MgCl<sub>2</sub>, 5  $\mu$ Ci [<sup>32</sup>P]ATP, and 10  $\mu$ M ATP) in 25- $\mu$ l volumes. The mixture was incubated at 30°C for 30 min, and the reaction was stopped by the addition of the LDS sample buffer (Thermo Fisher). The samples were run on an SDS-PAGE gel, which was stained with Coomassie Brilliant Blue R-250 (Bio-Rad) and subsequently dried and used for autoradiography using a phosphorimager screen. The signal was detected by an FLA 7000 scanner (GE Healthcare).

## Crystallization of *Trypanosoma congolense* KKT2<sup>1030–1265</sup> and *Trypanosoma brucei* KKT3<sup>847–1058</sup>

All crystals were obtained in sitting drop vapor diffusion experiments in 96-well plates, using drops of overall volume 200 nl, mixing protein and mother liquor in a 1:1 ratio except for SeMet *T. brucei* KKT3<sup>847–1058</sup>, which was optimized in a sitting drop vapor diffusion experiment in 48-well plate using drops of overall volume 400 nl, mixing protein and mother liquor in a 3:1 ratio. Crystals of *T. congolense* KKT2<sup>1030–1265</sup> (10.7 mg/ml) were grown at 4°C in a MIDAS HT-96 B5 solution (Molecular Dimensions) containing 0.1 M HEPES, pH 7.0, 8% wt/vol polyvinyl alcohol, 10% vol/vol 1-propanol. Crystals were briefly transferred into mother liquor prepared with the addition of 25% glycerol before flash-cooling by plunging into liquid nitrogen. Crystals of native *T. brucei* KKT3<sup>847–1058</sup> (12.2 mg/ml) were grown at 4°C in 25% PEG3350, 0.1 M Bis-Tris pH 5.5, and 0.1 M tri-sodium acetate pH 4.5. The crystals were briefly transferred into a cryoprotecting solution supplemented with 15% glycerol before flash cooling. Crystals of SeMet *T. brucei* KKT3<sup>847–1058</sup> (18.6 mg/ml) were grown at 4°C in 27% PEG3350 and 0.05 M Bis-Tris pH 5.5. The crystals were briefly transferred into a cryoprotecting solution of 35% PEG3350 and 0.05 M Bis-Tris pH 5.5 before flash cooling.

## Diffraction data collection and structure determination

X-ray diffraction data from *T. congolense* KKT2<sup>1030–1265</sup> were collected at the i03 beamline at the Diamond Light Source (Harwell, UK). The structure was solved using PHASER (McCoy, 2017), a molecular replacement program, with the AlphaFold2-predicted structure of *T. congolense* KKT2<sup>1030–1265</sup> as a model. Following the molecular replacement, the initial model building was done with BUCCANEER (Cowtan, 2006). Further manual model building and refinement were completed iteratively using COOT (Emsley et al., 2010) and PHENIX (Liebschner et al., 2019). Before the final refinement, the data were scaled to 2.2-Å resolution.

SeMet *T. brucei* KKT3<sup>847–1058</sup> X-ray diffraction data were collected at the I04 beam line at Diamond Light Source at the selenium K-edge wavelength (0.9795 Å) and processed using the Xia2 pipeline (Winter, 2010), with DIALS for indexing and integration (Winter et al., 2018) and AIMLESS for scaling to 2.13 Å (Evans and Murshudov, 2013). Initial phases and model were obtained with the Big EP pipeline (Sikharulidze et al., 2016) using autoSHARP (Vonrhein et al., 2007), Phenix AutoSol (Terwilliger et al., 2009), and Crank2

(Skubák and Pannu, 2013). The structure was then completed by using BUCCANEER (Cowtan, 2006) followed by alternate cycles of model building in Coot and refinement in autoBUSTER (Blanc et al., 2004; Bricogne et al., 2017). Native *T. brucei* KKT3<sup>847–1058</sup> X-ray diffraction data were collected at the I24 beam line at Diamond Light Source and processed using the Xia2 pipeline, with DIALS for indexing and integration and AIMLESS for scaling to 2.92 Å. Initial phases have been determined by molecular replacement with PHASER using a SeMet *T. brucei* KKT3<sup>847–1058</sup> structure as search model. The structure was completed with alternate cycles of model building in Coot and refinement in autoBUSTER. All images were made with PyMOL (version 2.5, Schrödinger). Protein coordinates have been deposited in the RCSB protein data bank with accession numbers 8A0J (*T. congolense* KKT2 DPB) and 8A0K (*T. brucei* KKT3 DPB).

## ACKNOWLEDGMENTS

We thank the crystallography facility manager Edward Lowe, Micron Advanced Bioimaging Unit, Advanced Proteomics Facility in Oxford, and the proteomics core facility at EMBL, especially Mandy Rettel and Jennifer Schwarz, for their support. We also thank Miguel Navarro (Instituto de Parasitología y Biomedicina López-Neyra, Consejo Superior de Investigaciones Científicas, Spain) for providing the pMig75 plasmid, Song Tan (Department of Biochemistry and Molecular Biology, Pennsylvania State University) for the pST44 plasmid, and Sam Dean (Warwick Medical School, University of Warwick, UK) for pPOT plasmids. M. Ishii was supported by a long-term fellowship from the TOYOBO Biotechnology Foundation. P. Ludzia was supported by the Boehringer Ingelheim Fonds. B. Akiyoshi was supported by a Wellcome Trust Senior Research Fellowship (Grant 210622/Z/18/Z) and the European Molecular Biology Organization Young Investigator Program.

## REFERENCES

- Akiyoshi B, Gull K (2014). Discovery of unconventional kinetochores in kinetoplastids. *Cell* 156, 1247–1258.
- Archer SK, Inchaustegui D, Queiroz R, Clayton C (2011). The cell cycle regulated transcriptome of *Trypanosoma brucei*. *PLoS ONE* 6, e18425.
- Ashkenazy H, Abadi S, Martz E, Chay O, Mayrose I, Pupko T, Ben-Tal N (2016). ConSurf 2016: an improved methodology to estimate and visualize evolutionary conservation in macromolecules. *Nucleic Acids Res* 44, W344–W350.
- Aslett M, Aurrecochea C, Berriman M, Brestelli J, Brunk BP, Carrington M, Depledge DP, Fischer S, Gajria B, Gao X, et al. (2010). TriTrypDB: a functional genomic resource for the Trypanosomatidae. *Nucleic Acids Res* 38, D457–D462.
- Berriman M, Ghedin E, Hertz-Fowler C, Blandin G, Renauld H, Bartholomeu DC, Lennard NJ, Caler E, Hamlin NE, Haas B, et al. (2005). The genome of the African trypanosome *Trypanosoma brucei*. *Science* 309, 416–422.
- Bieniossek C, Imasaki T, Takagi Y, Berger I (2012). MultiBac: expanding the research toolbox for multiprotein complexes. *Trends Biochem Sci* 37, 49–57.
- Bishop AC, Ubersax JA, Petsch DT, Matheos DP, Gray NS, Blethrow J, Shimizu E, Tsien JZ, Schultz PG, Rose MD, et al. (2000). A chemical switch for inhibitor-sensitive alleles of any protein kinase. *Nature* 407, 395–401.
- Blanc E, Roversi P, Vonrhein C, Flensburg C, Lea SM, Bricogne G (2004). Refinement of severely incomplete structures with maximum likelihood in BUSTER-TNT. *Acta Crystallogr D Biol Crystallogr* 60, 2210–2221.
- Bricogne G, Blanc E, Brandl M, Flensburg C, Keller P, Paciorek W, Roversi P, Sharff A, Smart OS, Vonrhein C, Womack TO (2017). BUSTER version 2.10.3. Cambridge, United Kingdom: Global Phasing.
- Brun R, Schönenberger M (1979). Cultivation and in vitro cloning or pro-cyclic culture forms of *Trypanosoma brucei* in a semi-defined medium. Short communication. *Acta Trop* 36, 289–292.
- Brusini L, D'Archivio S, McDonald J, Wickstead B (2021). Trypanosome KKI1 dynamically links the inner kinetochore to a kinetoplastid outer kinetochore complex. *Front Cell Infect Microbiol* 11, 641174.

- Butenko A, Oppendoerfer FR, Flegontova O, Horák A, Hampl V, Keeling PJ, Gawryluk RMR, Tikhonenkov D, Flegontov P, Lukeš J (2020). Evolution of metabolic capabilities and molecular features of diplomonads, kinetoplastids, euglenids. *BMC Biol* 18, 23.
- Chen Z-L, Meng J-M, Cao Y, Yin J-L, Fang R-Q, Fan S-B, Liu C, Zeng W-F, Ding Y-H, Tan D, et al. (2019). A high-speed search engine pLink 2 with systematic evaluation for proteome-scale identification of cross-linked peptides. *Nat Commun* 10, 3404.
- Combe CW, Fischer L, Rappsilber J (2015). xiNET: cross-link network maps with residue resolution. *Mol Cell Proteomics* 14, 1137–1147.
- Cowtan K (2006). The Buccaneer software for automated model building. 1. Tracing protein chains. *Acta Crystallogr D Biol Crystallogr* 62, 1002–1011.
- Cox J, Mann M (2008). MaxQuant enables high peptide identification rates, individualized p.p.b.-range mass accuracies and proteome-wide protein quantification. *Nat Biotechnol* 26, 1367–1372.
- D'Archivio S, Wickstead B (2017). Trypanosome outer kinetochore proteins suggest conservation of chromosome segregation machinery across eukaryotes. *J Cell Biol* 216, 379–391.
- d'Avila-Levy CM, Boucinha C, Kostygov A, Santos HLC, Morelli KA, Grybchuk-Ieremenko A, Duval L, Votýpka J, Yurchenko V, Grellier P, Lukeš J (2015). Exploring the environmental diversity of kinetoplastid flagellates in the high-throughput DNA sequencing era. *Mem Inst Oswaldo Cruz* 110, 956–965.
- Dean S, Sunter J, Wheeler RJ, Hodkinson I, Gluenz E, Gull K (2015). A toolkit enabling efficient, scalable and reproducible gene tagging in trypanosomatids. *Open Biol* 5, 140197.
- Deutsch EW, Bandeira N, Sharma V, Perez-Riverol Y, Carver JJ, Kundu DJ, Garcia-Seisdedos D, Jarnuczak AF, Hewapathirana S, Pullman BS, et al. (2020). The ProteomeXchange consortium in 2020: enabling “big data” approaches in proteomics. *Nucleic Acids Res* 48, D1145–D1152.
- Drinnenberg IA, Akiyoshi B (2017). Evolutionary lessons from species with unique kinetochores. *Prog Mol Subcell Biol* 56, 111–138.
- Drinnenberg IA, deYoung D, Henikoff S, Malik HS (2014). Recurrent loss of CenH3 is associated with independent transitions to holocentricity in insects. *Elife* 3, e03676.
- Eddy SR (1998). Profile hidden Markov models. *Bioinformatics* 14, 755–763.
- Elia AEH, Rellos P, Haire LF, Chao JW, Ivins FJ, Hoepker K, Mohammad D, Cantley LC, Smerdon SJ, Yaffe MB (2003). The molecular basis for phosphodependent substrate targeting and regulation of Plks by the Polo-box domain. *Cell* 115, 83–95.
- Emsly P, Lohkamp B, Scott WG, Cowtan K (2010). Features and development of Coot. *Acta Crystallogr D Biol Crystallogr* 66, 486–501.
- Ericson M, Janes MA, Butter F, Mann M, Ullu E, Tschudi C (2014). On the extent and role of the small proteome in the parasitic eukaryote *Trypanosoma brucei*. *BMC Biol* 12, 14.
- Evans PR, Murshudov GN (2013). How good are my data and what is the resolution? *Acta Cryst D* 69, 1204–1214.
- Gascoigne KE, Cheeseman IM (2013). CDK-dependent phosphorylation and nuclear exclusion coordinately control kinetochore assembly state. *J Cell Biol* 201, 23–32.
- Geoghegan V, Jones NG, Dowle A, Mottram JC (2021). Protein kinase signalling at the *Leishmania* kinetochore captured by XL-BioID. 2021.07.08.451598. doi:10.1101/2021.07.08.451598.
- Gileadi O, Burgess-Brown NA, Colebrook SM, Berridge G, Savitsky P, Smea CEA, Loppnau P, Johansson C, Salah E, Pantic NH (2008). High throughput production of recombinant human proteins for crystallography. *Methods Mol Biol* 426, 221–246.
- Hayashi H, Akiyoshi B (2018). Degradation of cyclin B is critical for nuclear division in *Trypanosoma brucei*. *Biol Open* 7. doi:10.1242/bio.031609.
- Holm L (2020). DALI and the persistence of protein shape. *Protein Sci* 29, 128–140.
- Hutti JE, Jarrell ET, Chang JD, Abbott DW, Storz P, Tokar A, Cantley LC, Turk BE (2004). A rapid method for determining protein kinase phosphorylation specificity. *Nat Methods* 1, 27–29.
- Ishii M, Akiyoshi B (2020). Characterization of unconventional kinetochore kinases KKT10 and KKT19 in *Trypanosoma brucei*. *J Cell Sci* 133. doi:10.1242/jcs.240978.
- Ishii M, Akiyoshi B (2022). Plasticity in centromere organization and kinetochore composition: lessons from diversity. *Curr Opin Cell Biol* 74, 47–54.
- Jones NG, Thomas EB, Brown E, Dickens NJ, Hammarton TC, Mottram JC (2014). Regulators of *Trypanosoma brucei* cell cycle progression and differentiation identified using a kinome-wide RNAi screen. *PLoS Pathog* 10, e1003886.
- Jumper J, Evans R, Pritzel A, Green T, Figurnov M, Ronneberger O, Tunyasuvunakool K, Bates R, Zidek A, Potapenko A, et al. (2021). Highly accurate protein structure prediction with AlphaFold. *Nature* doi:10.1038/s41586-021-03819-2.
- Jurrus E, Engel D, Star K, Monson K, Brandi J, Felberg LE, Brookes DH, Wilson L, Chen J, Liles K, et al. (2018). Improvements to the APBS bio-molecular solvation software suite. *Protein Science* 27, 112–128.
- Katoh K, Rozewicki J, Yamada KD (2019). MAFFT online service: multiple sequence alignment, interactive sequence choice and visualization. *Brief Bioinformatics* 20, 1160–1166.
- Keeling PJ, Burki F (2019). Progress towards the tree of eukaryotes. *Curr Biol* 29, R808–R817.
- Kelly S, Reed J, Kramer S, Ellis L, Webb H, Sunter J, Salje J, Marinsek N, Gull K, Wickstead B, Carrington M (2007). Functional genomics in *Trypanosoma brucei*: a collection of vectors for the expression of tagged proteins from endogenous and ectopic gene loci. *Mol Biochem Parasitol* 154, 103–109.
- Landeira D, Navarro M (2007). Nuclear repositioning of the VSG promoter during developmental silencing in *Trypanosoma brucei*. *J Cell Biol* 176, 133–139.
- Liebschner D, Afonine PV, Baker ML, Bunkóczi G, Chen VB, Croll TI, Hintze B, Hung LW, Jain S, McCoy AJ, et al. (2019). Macromolecular structure determination using X-rays, neutrons and electrons: recent developments in Phenix. *Acta Crystallogr D Struct Biol* 75, 861–877.
- Llauro A, Hayashi H, Bailey ME, Wilson A, Ludzia P, Asbury CL, Akiyoshi B (2018). The kinetoplastid kinetochore protein KKT4 is an unconventional microtubule tip-coupling protein. *J Cell Biol* 217, 3886–3900.
- Lowell JE, Cross GAM (2004). A variant histone H3 is enriched at telomeres in *Trypanosoma brucei*. *J Cell Sci* 117, 5937–5947.
- Ludzia P, Lowe ED, Marciano G, Mohammed S, Redfield C, Akiyoshi B (2021). Structural characterization of KKT4, an unconventional microtubule-binding kinetochore protein. *Structure* 29, 1014–1028.e8.
- Marciano G, Ishii M, Nerusheva OO, Akiyoshi B (2021). Kinetoplastid kinetochore proteins KKT2 and KKT3 have unique centromere localization domains. *J Cell Biol* 220, e202101022.
- McAllister MR, Ikeda KN, Lozano-Núñez A, Anrather D, Unterwurzacher V, Gossenreiter T, Perry JA, Crickley R, Mercadante CJ, Vaughan S, de Graffenried CL (2015). Proteomic identification of novel cytoskeletal proteins associated with TbPLK, an essential regulator of cell morphogenesis in *Trypanosoma brucei*. *Mol Biol Cell* 26, 3013–3029.
- McCoy AJ (2017). Acknowledging errors: advanced molecular replacement with Phaser. *Methods Mol Biol* 1607, 421–453.
- McIntosh JR (2016). Mitosis. *Cold Spring Harb Perspect Biol* 8. doi:10.1101/cshperspect.a023218.
- Merritt C, Stuart K (2013). Identification of essential and non-essential protein kinases by a fusion PCR method for efficient production of transgenic *Trypanosoma brucei*. *Mol Biochem Parasitol* 190, 44–49.
- Mirdita M, Schütze K, Moriwaki Y, Heo L, Ovchinnikov S, Steinegger M (2022). ColabFold—making protein folding accessible to all. <https://doi.org/10.1101/2021.08.15.456425>.
- Musacchio A, Desai A (2017). A molecular view of kinetochore assembly and function. *Biology (Basel)* 6, 5.
- Navarro-Mendoza MI, Pérez-Arques C, Panchal S, Nicolás FE, Mondo SJ, Ganguly P, Pangilinan J, Grigoriev IV, Heitman J, Sanyal K, Garre V (2019). Early diverging fungus *Mucor circinelloides* lacks centromeric histone CENP-A and displays a mosaic of point and regional centromeres. *Curr Biol* 29, 3791–3802.e6.
- Nerusheva OO, Akiyoshi B (2016). Divergent polo box domains underpin the unique kinetoplastid kinetochore. *Open Biol* 6, 150206.
- Nerusheva OO, Ludzia P, Akiyoshi B (2019). Identification of four unconventional kinetoplastid kinetochore proteins KKT22–25 in *Trypanosoma brucei*. *Open Biol* 9, 190236.
- Nishino M, Choy JW, Gushwa NN, Osés-Prieto JA, Koupparis K, Burlingame AL, Renslo AR, McKerrow JH, Taunton J (2013). Hypothemycin, a fungal natural product, identifies therapeutic targets in *Trypanosoma brucei*. *Elife* 2, e00712.
- Parsons M, Ramasamy G, Vasconcelos EJR, Jensen BC, Myler PJ (2015). Advancing *Trypanosoma brucei* genome annotation through ribosome profiling and spliced leader mapping. *Mol Biochem Parasitol* 202, 1–10.
- Parsons M, Worthey EA, Ward PN, Mottram JC (2005). Comparative analysis of the kinomes of three pathogenic trypanosomatids: *Leishmania major*, *Trypanosoma brucei* and *Trypanosoma cruzi*. *BMC Genomics* 6, 127.
- Perez-Riverol Y, Csordas A, Bai J, Bernal-Llinares M, Hewapathirana S, Kundu DJ, Inuganti A, Griss J, Mayer G, Eisenacher M, et al. (2019). The PRIDE database and related tools and resources in 2019: improving support for quantification data. *Nucleic Acids Res* 47, D442–D450.
- Poon SK, Peacock L, Gibson W, Gull K, Kelly S (2012). A modular and optimized single marker system for generating *Trypanosoma brucei*

- cell lines expressing T7 RNA polymerase and the tetracycline repressor. *Open Biol* 2, 110037.
- Qian W-J, Park J-E, Grant R, Lai CC, Kelley JA, Yaffe MB, Lee KS, Burke TR (2015). Neighbor-directed histidine N ( $\tau$ )-alkylation: a route to imidazolium-containing phosphopeptide macrocycles. *Biopolymers* 104, 663–673.
- Robinson DR, Sherwin T, Ploubidou A, Byard EH, Gull K (1995). Microtubule polarity and dynamics in the control of organelle positioning, segregation, and cytokinesis in the trypanosome cell cycle. *J Cell Biol* 128, 1163–1172.
- Saldivia M, Fang E, Ma X, Myburgh E, Carnielli JBT, Bower-Lepts C, Brown E, Ritchie R, Lakshminarayana SB, Chen Y-L, et al. (2020). Targeting the trypanosome kinetochore with CLK1 protein kinase inhibitors. *Nat Microbiol* 5, 1207–1216.
- Saldivia M, Wollman AJM, Carnielli JBT, Jones NG, Leake MC, Bower-Lepts C, Rao SPS, Mottram JC (2021). A CLK1–KKT2 signaling pathway regulating kinetochore assembly in *Trypanosoma brucei*. *mBio* 12, e0068721.
- Savitski MM, Reinhard FBM, Franken H, Werner T, Savitski MF, Eberhard D, Molina DMartinez, Jafari R, Dovega RB, Klaeger S, et al. (2014). Tracking cancer drugs in living cells by thermal profiling of the proteome. *Science* 346, 1255784.
- Schneider CA, Rasband WS, Eliceiri KW (2012). NIH Image to ImageJ: 25 years of image analysis. *Nat Methods* 9, 671–675.
- Sikharulidze I, Winter G, Hall DR, IUCr (2016). Big EP: Automated structure solution pipeline deployment at Diamond Light Source. *Acta Crystallographica Section A: Foundations and Advances*. 72, s193–s193.
- Skubák P, Pannu NS (2013). Automatic protein structure solution from weak X-ray data. *Nat Commun* 4, 2777.
- Tanifuji G, Cenci U, Moog D, Dean S, Nakayama T, David V, Fiala I, Curtis BA, Sibbald SJ, Onodera NT, et al. (2017). Genome sequencing reveals metabolic and cellular interdependence in an amoeba–kinetoplastid symbiosis. *Sci Rep* 7, 11688.
- Terwilliger TC, Adams PD, Read RJ, McCoy AJ, Moriarty NW, Grosse-Kunstleve RW, Afonine PV, Zwart PH, Hung LW (2009). Decision-making in structure solution using Bayesian estimates of map quality: the PHENIX AutoSol wizard. *Acta Crystallogr D Biol Crystallogr* 65, 582–601.
- Tikhonenkov DV, Gawryluk RMR, Mylnikov AP, Keeling PJ (2021). First finding of free-living representatives of Prokinetoplastina and their nuclear and mitochondrial genomes. *Sci Rep* 11, 2946.
- Tromer EC, Wemyss TA, Ludzia P, Waller RF, Akiyoshi B (2021). Repurposing of synaptonemal complex proteins for kinetochores in Kinetoplastida. *Open Biol* 11, 210049.
- UniProt Consortium (2019). UniProt: a worldwide hub of protein knowledge. *Nucleic Acids Res* 47, D506–D515.
- van Hooff JJ, Tromer E, van Wijk LM, Snel B, Kops GJ (2017). Evolutionary dynamics of the kinetochore network in eukaryotes as revealed by comparative genomics. *EMBO Rep* 18, 1559–1571.
- Varadi M, Anyango S, Deshpande M, Nair S, Natassia C, Yordanova G, Yuan D, Stroe O, Wood G, Laydon A, et al. (2022). AlphaFold Protein Structure Database: massively expanding the structural coverage of protein-sequence space with high-accuracy models. *Nucleic Acids Res* 50, D439–D444.
- Vonrhein C, Blanc E, Roversi P, Bricogne G (2007). Automated structure solution with autoSHARP. *Methods Mol Biol* 364, 215–230.
- Waterhouse AM, Procter JB, Martin DMA, Clamp M, Barton GJ (2009). Jalview Version 2—a multiple sequence alignment editor and analysis workbench. *Bioinformatics* 25, 1189–1191.
- Wheeler RJ (2021). A resource for improved predictions of *Trypanosoma* and *Leishmania* protein three-dimensional structure. *PLoS One* 16, e0259871.
- Winter G (2010). xia2: an expert system for macromolecular crystallography data reduction. *J Appl Cryst* 43, 186–190.
- Winter G, Waterman DG, Parkhurst JM, Brewster AS, Gildea RJ, Gerstel M, Fuentes-Montero L, Vollmar M, Michels-Clark T, Young ID, et al. (2018). DIALS: implementation and evaluation of a new integration package. *Acta Cryst D* 74, 85–97.
- Yu Z, Liu Y, Li Z (2012). Structure–function relationship of the Polo-like kinase in *Trypanosoma brucei*. *J Cell Sci* 125, 1519–1530.
- Zitouni S, Nabais C, Jana SC, Guerrero A, Bettencourt-Dias M (2014). Polo-like kinases: structural variations lead to multiple functions. *Nat Rev Mol Cell Biol* 15, 433–452.